Mössbauer Study of Magnetic States of $KFeF_3$ and Implications for $RbFeF_3$

G. R. Davidson,*† M. Eibschütz, and H. J. Guggenheim
Bell Telephone Laboratories, Murray Hill, New Jersey 07974
(Received 12 February 1973)

Mössbauer absorption spectra of ^{57}Fe in an unstrained {100} single-crystal platelet of $KFeF_3$ have been measured between 297 and 4.2 °K. The transition to the trigonal antiferromagnetic state occurred at $T_N = 112.5 \pm 0.5$ °K. The relaxation effects reported near T_N in a previous study were absent, but spectra of a strained crystal provided evidence of strong magnetoelastic interactions. A transition to a lower-symmetry weak ferromagnetic phase was found at $T_R = 36.6 \pm 0.5$ °K. At 4.2 °K the magnetic hyperfine field is $H_{hf} = 182.4 \pm 0.5$ kOe, and the magnitude of the quadrupole splitting is $|\Delta E_Q| = 1.97 \pm 0.05$ mm/sec. Analysis of the data in the antiferromagnetic phase indicates the spin alignment is parallel to the ⟨111⟩ distortion. The temperature dependence of H_{hf} and ΔE_Q in this phase is compared with predictions of self-consistent molecular-field-theory calculations. Only fair agreement is found with the magnetically induced electric-field-gradient (EFG) model, which describes the Fe^{2+} ions by a Hamiltonian incorporating free-ion terms, a cubic crystal field, and an exchange interaction. A substantially better fit is obtained with a second model which adds to this Hamiltonian an axial distortion term $(\delta/3)(L_z^2 - 2)$, where δ is zero above T_N and varies below T_N as $(1 - T/T_N)^\gamma$, with $\gamma = 1/2$ or $1/3$. Application of this second model to the tetragonal antiferromagnetic state of $RbFeF_3$ indicates that the spins align parallel to a ⟨100⟩ direction rather than the ⟨111⟩ direction predicted previously by use of the magnetically induced EFG model. The sign obtained for the axial-distortion parameter δ in $RbFeF_3$ is inconsistent with an analysis which attributes the cubic-to-axial transformation to Jahn-Teller stabilization effects.

I. INTRODUCTION

$KFeF_3$ and $RbFeF_3$ are two similar perovskites which have a low-temperature antiferromagnetic state with only a slight axial distortion (~0.3%) from cubic symmetry (along a ⟨111⟩ direction for $KFeF_3$ and a ⟨100⟩ direction for $RbFeF_3$).

Two properties make a Mössbauer-effect study of this state particularly interesting. First, the high symmetry of the Fe^{2+} site reduces the number of unknown parameters in any mathematical model of the system, thereby facilitating detailed interpretation of the data. Second, despite the smallness of the distortion, a sizable electric field gradient (EFG) has been observed at ^{57}Fe nuclei in previous Mössbauer-effect studies of the antiferromagnetic states of $KFeF_3$[1,2] and $RbFeF_3$.[3-5]

The origin of this EFG is still unresolved. Several investigators[1-3,5,6] have suggested that this EFG results primarily from effects of the long-range magnetic order. In this model of a magnetically induced EFG (MIEFG),[7] the Fe^{2+} ion is described by a Hamiltonian which includes free ion terms, a cubic crystal field, and an exchange interaction. While the MIEFG model can account for qualitative features of the Mössbauer spectra and yields approximate agreement with the temperature dependence of the EFG, two considerations make its applicability to $KFeF_3$ and $RbFeF_3$ questionable. First, estimates indicate that the distortion-induced crystal-field terms which are neglected in the MIEFG treatment are comparable in magnitude to the terms included. (These estimates are based on a measurement[8] of the magnetoelastic tensor G_{ij} of Fe^{2+} impurities in $KMgF_3$.[9,10]) Second, the MIEFG model leads to the prediction of a puzzling difference in magnetic behavior between these otherwise quite similar materials, the prediction that in $KFeF_3$ the spins align parallel to the axial distortion while in $RbFeF_3$ they align at an angle of ~55° to the distortion.

In the present work we report a study of the ^{57}Fe Mössbauer absorption spectra of an unstrained single crystal of $KFeF_3$ between room temperature and 4.2 °K. A major motivation of this work was to investigate the problem of the origin of the EFG. $KFeF_3$ was chosen because its antiferromagnetism persists over a temperature range much larger than that of $RbFeF_3$. An unstrained single crystal was used to circumvent the line-broadening problems which plagued previous Mössbauer studies of $KFeF_3$ and $RbFeF_3$ (in which powder samples were used) and prevented accurate determination of hyperfine parameters near the Néel point T_N. Our measurements constitute a substantial extension of the temperature range of Mössbauer spectroscopy in $KFeF_3$ since previously published measurements extend down to only 77 °K.

An attempt to fit the temperature dependence of our data for the antiferromagnetic state of $KFeF_3$ has led us to a reinterpretation of the origin of the EFG. In a later section we will show that addition of a temperature-dependent axial distortion term to the MIEFG Hamiltonian both produces a substantial-

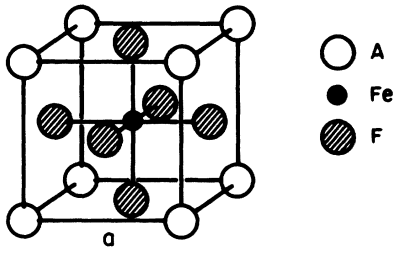

FIG. 1. Unit cell of $AFeF_3$, A = K or Rb, at room temperature.

ly better fit to the experimental data and eliminates the inconsistency in spin direction behavior between $KFeF_3$ and $RbFeF_3$. Treatment of $RbFeF_3$ with this augmented Hamiltonian leads us to question a model which attributes the cubic-to-axial transformation in these materials to Jahn-Teller stabilization effects.[11]

Our experimental results clarify other properties of $KFeF_3$. Well below T_N we discovered a phase transition to a lower-symmetry structure and explored its properties. We also encountered evidence of strong magnetoelastic interactions in the antiferromagnetic state.

Before proceeding, we review relevant results of previous studies of $KFeF_3$ and $RbFeF_3$. At room temperature both have the space group $Pm3m$ and the unit cell shown in Fig. 1.[12-17] The room-temperature lattice constants are $a = 4.121$ Å[13] and 4.174 Å[17] for $KFeF_3$ and $RbFeF_3$, respectively. For $KFeF_3$ values of 112 to 121 °K have been reported for T_N.[1,2,12,18,19] The trigonal structure below T_N is characterized by a rhombohedral angle α which decreases from 90° at T_N to 89°51′ at 78 °K.[13] For $RbFeF_3$ reported values of T_N range from 100.5 to 103 °K.[3,5,16,17] The tetragonal distortion at T_N leads to a c/a ratio of 1.0034 at 86 °K.[16] For both materials neutron-diffraction studies indicate that the antiferromagnetic ordering is G type with nearest-neighbor spins coupled antiparallel.[17,20] In both cases a single crystal develops a domain structure when cooled below T_N.[13,21] In $KFeF_3$ neighboring domains have their distortions along different ⟨111⟩ directions and all ⟨111⟩ distortion directions are equally probable.[13] The antiferromagnetic region in $RbFeF_3$ extends down to 86 °K, where it becomes ferrimagnetic; at 40 °K a transition to a weak ferromagnetic state occurs.[3,11,16,21] In $KFeF_3$ no transitions from the trigonal antiferromagnetic state were detected in studies extending down to 77 °K.

In Sec. II we describe our experimental technique. In Sec. III we present and analyze the resulting Mössbauer spectra. Section IV is devoted to an analysis of the temperature dependence of the hyperfine parameters obtained in the antiferromagnetic state of $KFeF_3$ and Sec. V to discussion of implications of our analysis. We summarize our findings in Sec. VI.

II. EXPERIMENT

Single crystals of $KFeF_3$ were grown from a stoichiometric mixture of FeF_2 and KF using the horizontal zone method. The FeF_2 was prepared by reacting 99.999% Fe sponge with dry HF at 900 °C. Zone-refined single crystals of KF were used.

Our temperature-dependence data were taken with a 3×8 mm {100} single-crystal platelet which was polished to a thickness of 0.1 mm. Strain-free mounting was achieved by placing the platelet inside a slightly larger cavity in a disk-shaped Lucite sample holder.

Temperatures of 77.4, 20.3, and 4.2 °K were obtained with the sample holder immersed in a cryogenic liquid. Other temperatures were obtained with the sample holder mounted in a Dewar vacuum space on a "cold finger" connected to the liquid reservoir by a thermal resistance. In the latter case temperature was measured by a platinum resistance thermometer[22] mounted near the sample. A germanium resistance thermometer[23] was used as a sensor for an automatic temperature controller which controlled the current to a heater on the cold finger. Fluctuations in the temperature of the platinum resistor during runs of ~24 h were always under ±0.05 °K. Despite careful radiation shielding, the spectra provided evidence (to be discussed later) of a temperature gradient possibly as large as 0.2 °K across the sample. We estimate that our platinum resistor provided a measure of the average sample temperature accurate to ±0.5 °K.

An electromechanical velocity drive of standard design was used.[24] Our source was ^{57}Co in Pd. The ground-state splitting of Fe foil, as recently remeasured by Violet and Pipkorn,[25] was used for calibration.

III. RESULTS AND PRELIMINARY ANALYSIS

Representative ^{57}Fe absorption spectra for the unstrained single crystal are shown in Fig. 2. These were taken with the γ radiation directed perpendicular to the {100} platelet. We label the three types of patterns observed I, II, and III in order of decreasing temperature. Parameters obtained for the single crystal with the fitting procedure described below are summarized in Tables I and II and plotted in Figs. 3 and 4.

A. Type-I Spectra

Single-line absorption spectra were observed at high temperatures. The linewidths [full width at

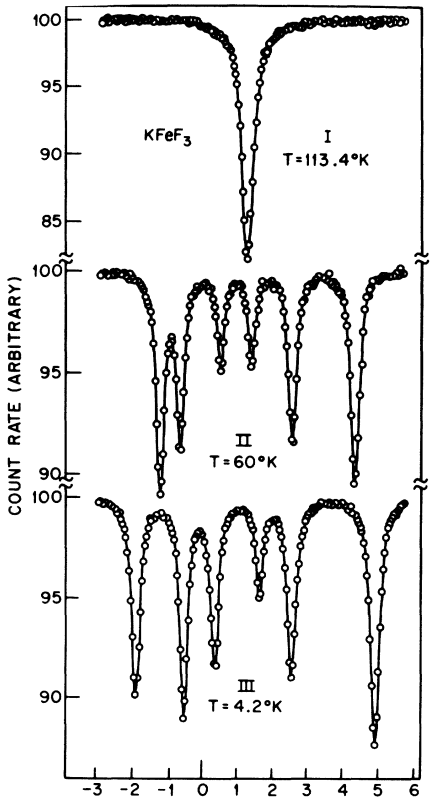

FIG. 2. Representative ^{57}Fe Mössbauer absorption spectra for an unstrained $KFeF_3$ single crystal. The solid lines are obtained by least-squares fits of the data to sums of Lorentzian curves.

half-maximum (FWHM) = 0.33 mm/sec at room temperature, 0.38 mm/sec at 125 °K] are somewhat higher than we observed for 1-mil Fe foil (0.29 mm/sec for the outer lines at room temperature). This line broadening is indicative of a Debye temperature of ~250±100 °K for $KFeF_3$, comparable to the Einstein temperature of 413±60 °K determined from thermal shift measurements.[26] Thus the spectra are consistent with the absence of unresolved hyperfine splitting and with the equivalence of all Fe sites, as expected for an undistorted paramagnetic perovskite.

B. Type-II Spectra

Type-II spectra reflect the combined presence of a magnetic hyperfine field and an electric field gradient.

Each type-II spectrum was fitted to a sum of six Lorentzian curves of independent position, width, and dip. Except for temperatures very near transition points, the resulting area-weighted average of the six linewidths of each spectrum was in the range 0.28±0.01 mm/sec, indicating nearly equivalent surroundings for all Fe nuclei.

The Hamiltonian of the $I=\frac{3}{2}$ excited state of ^{57}Fe may be written as[27,28]

$$\mathcal{H}_1 = g_1\mu_N H_{hf} I_z + \tfrac{1}{4}e^2qQ\left[I_{z'}^2 - \tfrac{5}{4} + \tfrac{1}{3}\eta(I_{x'}^2 - I_{y'}^2)\right], \quad (1)$$

where x', y', and z' are the principal axes of the EFG tensor V_{ij}, z is the direction of the magnetic hyperfine field $\vec{H}_{hf}$, and the other parameters have their usual meanings. As in the previous powder measurements,[1,2] the pattern of line positions in type-II spectra appeared to be close to that expected

TABLE I. Values for magnetic hyperfine field, quadrupole splitting, and center shift obtained for unstrained $KFeF_3$ single crystal at various temperatures.

T[a] (°K)	H_{hf}[b] (kOe)	$\lvert\Delta E_Q\rvert$[c] (mm/sec)	CS[d] (mm/sec)
297±2 °K	0	0	1.331
112.02	53.8	0.014	1.440
111.61	63.5	0.018	1.441
111.06	73.1	0.026	1.439
110.54	80.2	0.031	1.441
110.07	85.9	0.042	1.437
109.55	91.2	0.049	1.441
109.05	95.8	0.055	1.441
108.55	99.8	0.064	1.438
108.06	103.3	0.069	1.437
107.02	110.0	0.082	1.438
106.07	115.6	0.092	1.441
104.97	121.3	0.105	1.440
102.57	131.0	0.136	1.441
100.00	139.6	0.166	1.440
94.01	153.7	0.232	1.442
86.05	165.0	0.319	1.445
77.5±0.2	171.2	0.408	1.447
69.98	173.4	0.492	1.451
60.03	171.8	0.598	1.453
50.06	167.0	0.691	1.456
39.98	159.8	0.784	1.457
37.97[e]	158.1	0.798	1.453
36.74[e]	157.2	0.800	1.452
36.59[e]	161.7	1.20	1.457
36.52[e]	162.1	1.20	1.454
35.97	163.7	1.28	1.456
32.02	168.9	1.58	1.456
26.91	173.8	1.75	1.455
20.3±0.1	178.4	1.89	1.455
4.2±0.1	182.4	1.97	1.452

[a]Temperatures for which uncertainties are not stated varied by less than ± 0.05 °K during a measurement; their estimated accuracy is ± 0.5 °K.

[b]H_{hf} is magnitude of magnetic hyperfine field. Estimated uncertainty is ± 0.5 kOe.

[c]ΔE_Q is quadrupole splitting $(\frac{1}{2}e^2qQ)(1+\frac{1}{3}\eta^2)^{1/2}$. Above $T_R = 36.60$ °K, ΔE_Q is positive and estimated uncertainty is ± 0.006 mm/sec. Below T_R the sign of ΔE_Q was not determined; estimated uncertainty is ± 0.05 mm/sec.

[d]CS is center shift relative to Fe foil. Estimated uncertainty is ± 0.006 mm/sec.

[e]A superposition of two types of spectra is observed at this temperature. The parameters given here apply to the major portion by area.

TABLE II. Averages of values found below $T_R = 36.60$°K for η, θ, and φ of an unstrained $KFeF_3$ single crystal by use of Monte Carlo search program (Ref. 31). Uncertainties indicate spread of values consistent with the data (see text, Sec. III C, and Ref. 31).

	(a) If ΔE_Q positive[a]			(b) If ΔE_Q negative[a]		
T[b] (°K)	η	θ (deg)	φ (deg)	η	θ (deg)	φ (deg)
36.59[c]	0.56 ± 0.18	23.7 ± 2.8	48 ± 42	0.998 ± 0.006	72.2 ± 0.5	85 ± 5
36.52[c]	0.58 ± 0.17	24.3 ± 2.6	37 ± 27	0.996 ± 0.008	72.0 ± 0.4	85 ± 4
35.97[c]	0.58 ± 0.17	26.0 ± 2.2	35 ± 28	0.999 ± 0.004	70.5 ± 0.2	89 ± 4
32.02	0.56 ± 0.23	31.0 ± 2.3	30 ± 29	0.94 ± 0.05	68.2 ± 0.2	79 ± 5
26.91	0.53 ± 0.18	34.0 ± 1.6	36 ± 37	0.92 ± 0.08	67.1 ± 0.3	76 ± 7
20.3 ± 0.1	0.56 ± 0.22	36.4 ± 1.6	34 ± 30	0.81 ± 0.12	66.0 ± 0.5	73 ± 7
4.2 ± 0.1	0.54 ± 0.25	38.6 ± 1.6	33 ± 29	0.78 ± 0.14	65.0 ± 0.5	74 ± 11

[a]All results are based on χ^2 [Eq. (2)] < 1 except for three cases with $\Delta E_Q < 0$ ($T = 35.97$, 36.52, and 36.59°K). For these cases no $\chi^2 < 6$ was found. Results are for $\chi^2 < 10$.

[b]See Footnote a, Table I.

[c]See footnote e, Table I.

for the case of axial symmetry of $\mathcal{H}_1$, i.e., $z' = z$ and $\eta = 0$ in Eq. (1). We therefore analyzed these spectra assuming axial symmetry. With the absorption lines numbered 1 through 6 in order of increasing velocity, we determined H_{hf} from the ground-state splitting by the relation

$$g_0 \mu_N H_{hf} = \tfrac{1}{2}[(p_5 - p_3) + (p_4 - p_2)] ,$$

where p_j is the position of the jth absorption line. The center shift (CS) (the sum of the isomer shift and the second-order Doppler shift) was obtained by

$$CS = \tfrac{1}{4}(p_1 + p_2 + p_5 + p_6)$$

and the quadrupole splitting $\Delta E_Q = \frac{1}{2} e^2 q Q$ by

$$\tfrac{1}{2} e^2 q Q = \tfrac{1}{2}[(p_6 - p_5) - (p_2 - p_1)] .$$

We found ΔE_Q to be positive.

To test the validity of the hypothesis of axial symmetry, we used the above values for H_{hf}, CS, and $\frac{1}{2} e^2 q Q$ to calculate the line positions predicted by use of Eq. (1) with $z' = z$ and $\eta = 0$. The rms difference between the calculated and experimental positions was ~±0.003 mm/sec, an amount somewhat larger than the rms statistical uncertainty of the experimental positions (~±0.002 mm/sec). It is reasonable to attribute such a small discrepancy to nonlinearity in the velocity drive.

The relative line intensities provide further sup-

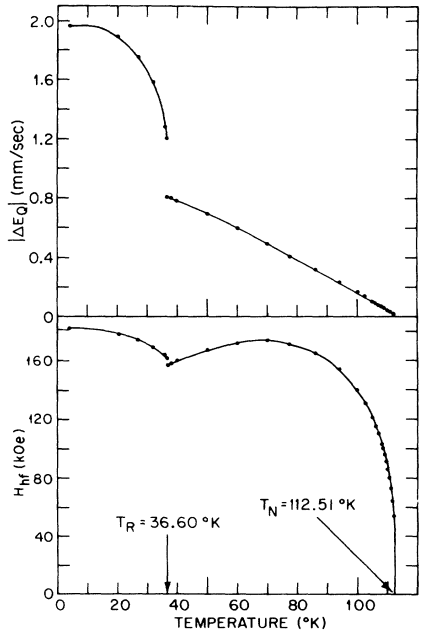

FIG. 3. Temperature dependence of magnitudes of magnetic hyperfine field (H_{hf}) and electric quadrupole splitting ($|\Delta E_Q|$) for ^{57}Fe in single crystal $KFeF_3$. The solid lines represent visual fits to the data.

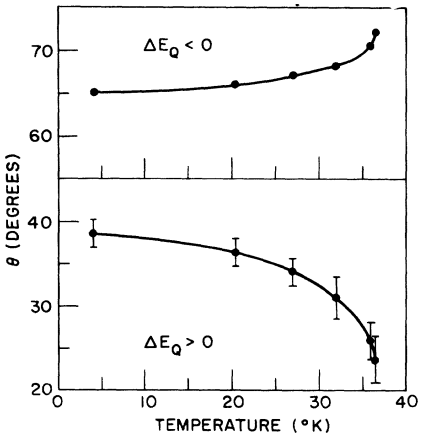

FIG. 4. Temperature dependence below T_R for θ, the polar angle of $\vec{H}_{hf}$ in the EFG principal axis system. The value found for θ depends on the sign assumed for the quadrupole splitting ΔE_Q. The solid lines are visual fits to the data.

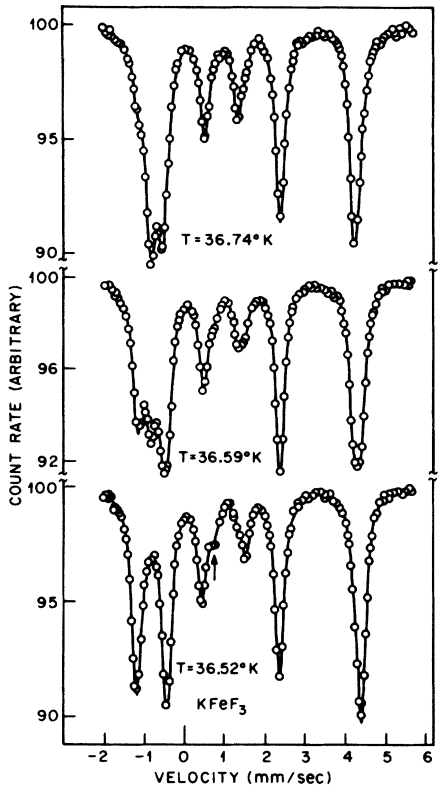

FIG. 5. Spectra in the vicinity of the transition at T_R. The solid lines are obtained by linear superposition of spectra of types II and III. The arrow (bottom spectrum) indicates a seventh resolved line.

port for the hypothesis of axial symmetry. The observed intensities are characteristic of a 3:2:1:1:2:3 pattern. Such a pattern is obtained for the case of axial symmetry and any of several conceivable distributions of spin directions. One possibility is that the Fe^{2+} spins point along one or more of the $\langle 111\rangle$ directions. Another way of obtaining the same intensity distribution is to have equal numbers of spins point along each of a set of directions equivalent by cubic symmetry, e.g., all of the $\langle 100\rangle$ directions.[29]

In summary, type-II spectra indicate H_{hf} and ΔE_Q are nonzero, $\eta = 0$, and $\vec{H}_{hf}$ is parallel to the principal axis of V_{ij}. These properties are consistent with previous findings that $KFeF_3$ transforms to a trigonal antiferromagnetic state when cooled.

C. Type-III Spectra

Spectra below a temperature T_R differ radically from those of type II in the pattern of line spacings and intensities. At some temperatures a seventh line is resolved. (See the bottom spectrum of Fig. 5.) These features indicate violation of one or both of the conditions $\eta = 0$ and $z' = z$.

For this case eight absorption transitions are possible. Their energies are determined by the center shift, the ground-state splitting $g_0\mu_N H_{hf}$, and the excited-state energies $E_i (i = 1, 2, 3, 4)$. Because $\sum_{i=1}^{4} E_i = 0$, the four excited-state energies may be specified by three splitting parameters: $S_1 \equiv E_1 - E_2$, $S_2 \equiv E_2 - E_3$, and $S_3 \equiv E_3 - E_4$. The splittings S_i can be calculated by diagonalization of $\mathcal{H}_1$ if five parameters are specified: H_{hf}, the quadrupole splitting $\Delta E_Q \equiv (\frac{1}{2} e^2 qQ)\,(1 + \frac{1}{3}\eta^2)^{1/2}$, η, and the polar and azimuthal angles θ and φ of $\vec{H}_{hf}$ in the $x'y'z'$ principal-axis coordinate system.

The first step in our analysis of each type-III spectrum was to make a least-squares fit to a sum of eight Lorentzian curves. To ensure convergence, we took as free parameters the CS, $g_0\mu_N H_{hf}$, and the three S_i rather than the eight line positions. The percent dip of each line and the widths of the six most intense lines were also free parameters. The widths of the two remaining lines were constrained to be equal to the average width of the middle pair of the six most prominent lines. The area-weighted averages of the linewidths were again in the range 0.28 ± 0.01 mm/sec, indicating that all Fe^{2+} sites are still nearly equivalent. From the splittings S_1, S_2, and S_3, we calculated the excited state energies E_i and used these to evaluate $|\Delta E_Q|$ by the formula given by Karyagin[30]:

$$|\Delta E_Q| = \left[\left(\sum_{i=1}^{4} E_i^2\right) - 5g_1^2\mu_N^2 H_{hf}^2\right]^{1/2}.$$

With H_{hf} and $|\Delta E_Q|$ fixed, we then searched for values of η, θ, and φ which would yield calculated splittings S_i^{calc} consistent with the observed splittings S_i and their uncertainties ΔS_i. The search was made by a Monte Carlo method with a computer program[31] which in effect made a quasirandom sampling of the distribution of those (η, θ, φ) parameters yielding values of

$$\chi^2 \equiv \frac{1}{3}\sum_{i=1}^{3}\left(\frac{(S_i^{calc} - S_i)}{\Delta S_i}\right)^2 \qquad (2)$$

lower than a specified value χ_0^2. Only line-energy information was used in the search as we found that sets of parameters which gave low χ^2 values led to nearly identical line intensity predictions. These predictions were consistent with the intensities we observed in Mössbauer spectra of $KFeF_3$ powder.

Table II summarizes the results of searches over the intervals $0 \le \eta \le 1$, $0 \le \theta \le 90°$, and $0 \le \varphi \le 90°$.[32] For each spectrum we found about 30 acceptable sets (η, θ, φ) yielding $\chi^2 < \chi_0^2$. (We used $\chi_0^2 = 1$ except for certain spectra near T_R where a slight admixture of lines from type-II spectra was present; see next section.) The parameter values and uncertainties $(\pm r)$ in Table II represent averages and rms deviations (r) of members in these

sets.

Good fits to the experimental data were found with both signs of ΔE_Q. For both signs θ was the best-defined parameter. Its variation with temperature is shown in Fig. 4. For $\Delta E_Q > 0$, η and φ are not well defined. If $\Delta E_Q < 0$, η is in general close to unity and φ close to 90°.

Attempts to obtain good fits with η fixed at zero were not successful with either sign of ΔE_Q. For the 4.2 °K spectrum we were unable to obtain a fit yielding $\chi^2 < 160$. This finding that $\eta \neq 0$ suggests that a structural change has occurred. This was confirmed by an x-ray diffraction study of a powder sample at 4.2 °K.[33] Line splitting indicative of a structure of symmetry lower than trigonal was observed.

A magnetic study at 4.2 °K showed $KFeF_3$ to be a weak ferromagnet.[34] A moment of 13.6 emu/g was obtained in an external field of 10 kOe. If we assume an Fe^{2+} moment of $4\mu_B$, this result indicates a canting of the spins by ~5°.

D. Transition Regions

The change in the spectral parameters that occurs at T_R is abrupt (see Fig. 5). Spectra close to T_R could be fitted quite well as a linear superposition of spectra of types II and III as indicated by the solid lines in Fig. 5. (To minimize the number of parameters in these fits, we assumed all lines to have the same width; values in the range 0.28 ± 0.01 mm/sec were found.) To estimate T_R, we plotted against temperature the fractional area of each type of pattern. The plot indicated that a 50%-50% mixture would occur with our platinum thermometer at 36.60 ± 0.02 °K, which we take as the value of T_R. The temperature difference separating spectra having 75%-25% and 25%-75% mixtures was 0.18 °K, a measure of the sum of the widths of two possible distributions, a temperature distribution across the sample or a distribution of T_R values. (The fact that we are studying a single crystal does not rule out the possibility of a spread in values of the transition temperature. A paramagnetic-to-antiferromagnetic transition ~5 °K broad has been observed in a Mössbauer study of an absorber made of single crystals of Rb_2FeF_4.[35])

The value of T_N was estimated by assuming the hyperfine field below T_N to have power-law dependence on temperature of the form

$$H_{hf} = C(1 - T/T_N)^{\beta} . \tag{3}$$

Such a behavior for H_{hf} at the nucleus of an Fe^{2+} ion has been previously observed.[3,36] From a least-squares fit to Eq. (3) with T_N, β, and C taken as free parameters, we obtained $T_N = 112.51 \pm 0.02$ °K, $\beta = 0.306 \pm 0.003$, and $C = 278 \pm 2$ kOe. Eleven data points corresponding to $0.933T_N \leq T \leq 0.991T_N$ were used in the fit. Calculated values agreed with experimental values to within ± 0.3%.

In their studies of a powder absorber of $KFeF_3$, Fatehally *et al.* observed below T_N pronounced line broadening, which they attributed to a slowing down of the Fe^{2+} relaxation rate as temperature is increased toward T_N.[37] In our measurements we found a slight line broadening which increased as T_N was approached. The average width W of the outer pair of lines was 0.28 mm/sec at 100.00 °K, and 0.36 mm/sec at 112.02 °K. This broadening could be due to relaxation effects, a temperature gradient, or a distribution in T_N values.

As a test of the second hypothesis we consider the relationship between W and a uniform temperature distribution of width ΔT. The temperature gradient produces a spread ΔH_{hf} in hyperfine field values:

$$\Delta H_{hf} \approx \left| \frac{dH_{hf}}{dT} \right| \Delta T .$$

The spread ΔH_{hf} causes an increase in the width of the outer lines of the order of $\gamma \Delta H_{hf}$ where

$$\gamma \equiv (1.5\,|g_1| + 0.5\,|g_0|)\mu_N$$
$$= 0.0161\,(\text{mm/sec})/\text{kOe} .$$

Thus,

$$W \approx W_0 + \gamma \left| \frac{dH_{hf}}{dT} \right| \Delta T , \tag{4}$$

where W_0 is a constant. Using our best fit to the power-law formula of Eq. (3) for calculation of dH_{hf}/dT, we made a least-squares fit of Eq. (4) to our data for W and found $\Delta T = 0.17$ °K.

If the line broadening were due to a spread ΔT_N in T_N values, a similar value would be obtained for ΔT_N by such a fit since $|dH_{hf}/dT_N| \approx |dH_{hf}/dT|$ for temperatures near T_N.

The closeness of our result for ΔT to the observed spread of ~0.18 °K near T_R suggests that similar mechanisms are operative in the two transition regions. Relaxation effects are clearly absent near T_R since no line broadening is observed. Hence, the line broadening near T_N is not due to relaxation effects.

E. Magnetoelastic and Other Effects

Indications of an extraordinary sensitivity of $KFeF_3$ to pressure were encountered in measurements made with a single-crystal {100} platelet that was held with an adhesive tape (Scotch-brand Mylar tape) to a Lucite disk. A pronounced alteration in relative line intensities at 100 °K was caused by the tape (Fig. 6). This change is indicative of a rotation of some of the spins away from their usual directions owing to strain induced by the difference between the thermal expansion coefficients of the sample and the tape. This result suggests that the spin directions are strongly

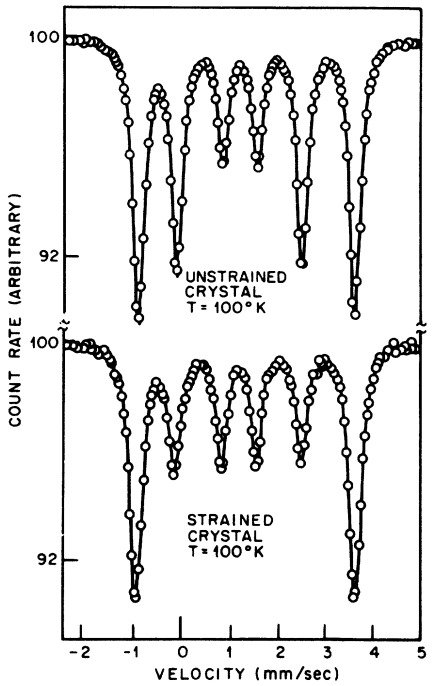

FIG. 6. Illustration of effects of strain on the Mössbauer spectrum of a single crystal. The change in line intensities indicates rotation of the spin directions.

coupled to the distortion direction, which is probably easily affected by external stress because of the smallness of the spontaneous distortion.[38]

Portions of the taped sample were found to have a higher value of T_N than an unstrained sample. This effect is illustrated by the middle spectrum in Fig. 7. The line broadening in the wings is evidence of magnetic hyperfine splitting at a temperature 1.5 °K above the T_N value of unstrained $KFeF_3$.

A similar rise and distribution of T_N values was observed in a powder sample and is shown in the bottom spectrum of Fig. 7. These effects are similar to those observed in Mössbauer spectra of powder $RbFeF_3$ by Wertheim *et al.*,[3] who attributed them to a strain-induced spatial variation of T_N. Our finding that stress can raise T_N lends support to their hypothesis.

IV. INTERPRETATION OF TEMPERATURE DEPENDENCE IN ANTIFERROMAGNETIC REGION

In the present section we will consider the temperature dependence of H_{hf} and ΔE_Q in the antiferromagnetic state of $KFeF_3$, where the crystallographic symmetry at the Fe^{2+} site is trigonal. We will attempt to fit the data to predictions of an Fe^{2+} electronic Hamiltonian based on the crystal-field and molecular-field approximations. No attempt will be made to fit data below T_R as the reduced symmetry there leads to a model with too many unknown parameters.

A. Mathematical Formalism

The free Fe^{2+} ion has an [Ar] $3d^6$ ground configuration and a ^5D ground term separated by about 20 000 cm^{-1} from the next highest term.[39,40] The octahedral cubic crystal field of $KFeF_3$ splits the ^5D level into an orbital triplet $^5T_{2g}$ and an orbital doublet ^5E_g higher by ~ 9000 cm^{-1}.[39,41] The ground state has spin 2 so its total degeneracy is $3\times 5 = 15$. The principal perturbations to the $^5T_{2g}$ state may be represented by the Hamiltonian[6,42]

$$\mathcal{H}' = \lambda \vec{L}\cdot\vec{S} + hS_z + \tfrac{1}{3}\delta(L_z^2 - 2)\,, \qquad (5)$$

where $\vec{L}$ and $\vec{S}$ are the total orbital and spin angular momenta of the ion and z denotes the ⟨111⟩ distortion direction. The first term in $\mathcal{H}'$ is due to spin-orbit coupling. The second is the Heisenberg exchange interaction treated in the molecular-field approximation. The third term is an approximate representation of the crystal field arising from the trigonal distortion.[43] We have assumed

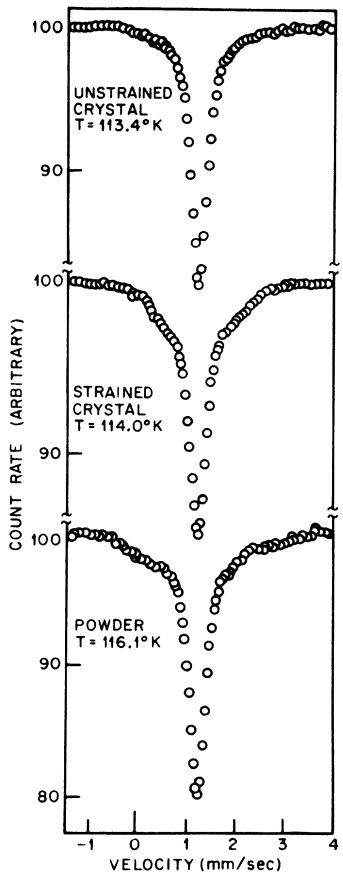

FIG. 7. Examples of effects of straining a crystal and powdering a crystal on spectra at temperatures above the T_N value of an unstrained crystal.

spin alignment parallel to the distortion. We will show later that any other assumption would be inconsistent with the Mössbauer data.

The EFG produced by $\mathcal{H}'$ at the nucleus of an ion will be axially symmetric. Its V_{zz} component may be expressed as[44,45]

$$V_{zz}/e \equiv q = (1-R)q_{\rm val} + (1-\gamma_\infty)q_{\rm lat} ,$$

where $q_{\rm val}$ is the EFG of the aspherical $3d$ valence electron of the ion and $q_{\rm lat}$ is the contribution of the remaining ions of the lattice. The factors $(1-R)$ and $(1-\gamma_\infty)$ account for Sternheimer shielding[45] by the [Ar] $3d^5$ core. Estimated values include 0.68 for $(1-R)$,[46] and 10.14 for $(1-\gamma_\infty)$.[47]

Calculation of $q_{\rm lat}$ for $KFeF_3$ is not possible because precise positional parameters are not available below T_N. However, because the contribution to V_{zz} from a charge at a distance r from the nucleus is proportional to $(1/r^3)$, it is reasonable to expect

$$(1-R)q_{\rm val} \gg (1-\gamma_\infty)q_{\rm lat} .$$

Several previous studies support this expectation. Nozik and Kaplan[48] have used the point-charge model to estimate lattice contributions to the ^{57}Fe quadrupole splitting ΔE_Q for four Fe^{2+} compounds. Their calculated lattice contributions range from 0.5% to 13.3% of the experimentally measured ΔE_Q. Also, in several cases good fits to the temperature dependence of ΔE_Q have been obtained with $q_{\rm lat}$ neglected.[49] We will therefore assume $q_{\rm lat}=0$ in our treatment.

Using operator equivalent formalism[42] and assuming sufficiently fast relaxation among the electronic states of the Fe^{2+} ion,[50] one may show that the valence contribution to V_{zz}/e can be written

$$(1-R)q_{\rm val} = \tfrac{2}{7}\langle r^{-3}\rangle_Q \langle L_z^2 - 2\rangle$$

The $3d$ radial parameter $\langle r^{-3}\rangle_Q$ includes the factor $(1-R)$. We use the unsubscripted brackets $\langle\cdots\rangle$ to denote a thermal expectation value; i.e., if M is an operator, its expectation value at a temperature T is

$$\langle M\rangle \equiv \frac{\sum_n \langle\Psi_n | M | \Psi_n\rangle e^{-E_n/kT}}{\sum_n e^{-E_n/kT}} ,$$

where Ψ_n and E_n are the electronic wave functions and energy levels. Since the ^{57}Fe quadrupole moment Q is positive,[51] the quadrupole splitting at a temperature T is a positive multiple of $\langle L_z^2 - 2\rangle$:

$$\Delta E_Q = \tfrac{1}{7}e^2 Q \langle r^{-3}\rangle_Q \langle L_z^2 - 2\rangle . \quad (6)$$

In the present case the principal contributions to the magnetic hyperfine field at an ^{57}Fe nucleus may be expressed as[6,52]

$$H_{\rm hf}^z = A\langle S_z\rangle + 2\mu_B\langle r^{-3}\rangle_L\langle L_z\rangle - \tfrac{1}{14}\mu_B\langle r^{-3}\rangle_L \times \langle \hbar_z^D\rangle , \quad (7)$$

where $h_z^D \equiv 4S_z - (\vec{L}\cdot\vec{S})L_z - L_z(\vec{L}\cdot\vec{S})$. The first of the terms on the right-hand side represents effects of the Fermi contact hyperfine field and the supertransferred hyperfine field.[52] The second term is the field due to the orbital angular momentum of the $3d$ electrons, and the last term is the dipolar field due to these electrons. In writing this expression we have assumed equality of the orbital and dipolar radial parameters $\langle r^{-3}\rangle_L$ and $\langle r^{-3}\rangle_D$.[53] Because of the threefold symmetry of the Fe^{2+} site, the x and y components of $\vec{H}_{\rm hf}$ must be zero. Note that we distinguish $H_{\rm hf} \equiv |\vec{H}_{\rm hf}|$ from $H_{\rm hf}^z$, which may be positive or negative depending on whether $\vec{H}_{\rm hf}$ is parallel or antiparallel to the ionic magnetic moment $\vec{\mu}$.

For calculation of Ψ_n and E_n, it is helpful to have estimates of the approximate sizes of the terms in $\mathcal{H}'$.

For a free Fe^{2+} ion, the spin-orbit coupling constant $\lambda = \lambda_0 \equiv -103\ {\rm cm}^{-1}$.[40] In a solid, covalency[54] and dynamic Jahn-Teller[55] effects may reduce $|\lambda|$ to as low as 50% of $|\lambda_0|$.

If each Fe^{2+} ion is assumed to have an exchange interaction that is isotropic and involves only its n nearest-neighbor Fe^{2+} ions, then the exchange parameter h is related to the exchange integral J by[56]

$$h = 2nJ\langle S_z\rangle ,$$

where $n=6$. The elementary molecular-field theory treatment of an isolated ion relates J to T_N by[56]

$$J = -3kT_N/2S(S+1) . \quad (8)$$

Using $T_N = 112.51\ ^\circ$K and $\langle S_z\rangle = 2$ leads to an estimate of $-78\ {\rm cm}^{-1}$ for the saturation value of h.

Finally, we may estimate δ on the basis of the magnetoelastic tensor[8,9] G_{ij} of Fe^{++} impurities in $KMgF_3$. It can be shown that δ is related to the strain parameter[57] ϵ_{12} by $\delta = 30G_{44}\epsilon_{12}$. The rhombohedral angle $\alpha = 89^\circ 51'$ of $KFeF_3$ at 78 °K yields $\epsilon_{12} = 1.31\times10^{-3}$. Using $|G_{44}| = 1000\pm100\ {\rm cm}^{-1}$,[8] we obtain $|\delta| = 39\pm4\ {\rm cm}^{-1}$.

Since $|\lambda|$, $|h|$, $|\delta|$, and kT for temperatures of interest are much smaller than Δ, the effects of $\mathcal{H}'$ may be treated by first-order perturbation theory applied to the $^5T_{2g}$ state. Because the magnitudes of λ, h, and δ are comparable, all terms in $\mathcal{H}'$ must be diagonalized simultaneously.

A convenient choice for the 15 $^5T_{2g}$ basis functions is the following:

$$\Phi_n = \varphi_l \chi_s ,$$

where $n = 1, 2, \ldots, 15$; $l = 1, 0, -1$; and $s = -2, -1, \ldots, 2$. Here, χ_s denotes an eigenfunction of the operator S_z with eigenvalue s (in units of $\hbar$). The φ_l are orbital functions[58]:

$$\varphi_1 = -(\tfrac{1}{3})^{1/2} d_1 - (\tfrac{2}{3})^{1/2} d_{-2} ,$$
$$\varphi_0 = d_0 , \qquad (9)$$
$$\varphi_{-1} = -(\tfrac{1}{3})^{1/2} d_{-1} + (\tfrac{2}{3})^{1/2} d_2 ,$$

where d_m is the spherical harmonic $Y_2^m(\theta, \varphi)$ defined with respect to [111] as the polar axis. One helpful feature of this set of functions is that matrix elements of $\vec{L}$ are related in a simple way to those of p functions [$p_m \equiv Y_1^m(\theta, \varphi)$]:

$$\langle \varphi_m | \vec{L} | \varphi_n \rangle = -\langle p_m | \vec{L} | p_n \rangle .$$

Also, in the φ_l basis the important operator $(L_z^2 - 2)$ has a simple matrix representation:

$$(L_z^2 - 2) = \begin{array}{c|ccc} & \varphi_1 & \varphi_0 & \varphi_{-1} \\ \hline \varphi_1 & 1 & 0 & 0 \\ \varphi_0 & 0 & -2 & 0 \\ \varphi_{-1} & 0 & 0 & 1 \end{array} . \qquad (10)$$

Finally, by ordering the Φ_n as listed in Table III, the 15×15 matrix of $\mathcal{H}'$ in the ${}^5T_{2g}$ basis is reduced to block diagonal form so that the largest matrix one must diagonalize is 3×3. (Each function $\varphi_l \chi_s$ is an eigenfunction of $J_z \equiv -L_z + S_z$ with eigenvalue $j \equiv l + s$; basis functions belonging to the same block have the same j value.)

Before proceeding, it is helpful to consider some simple examples which provide insight into the relationship between the parameters of our formalism and the resulting ^{57}Fe quadrupole splitting ΔE_Q. The special cases we shall examine are illustrated in Fig. 8.

TABLE III. Standard order adopted for basis functions used for diagonalization of $\mathcal{H}'$ [Eq. (5)] within the ${}^5T_{2g}$ basis. The basis functions are of the form $\Phi_n = \varphi_l \chi_s$, where the φ_l are defined by Eqs. (9) and χ_s is an eigenfunction of S_z with eigenvalue s (in units of $\hbar$). Also listed is the j value associated with each function ($j \equiv \langle \Phi_n | -L_z + S_z | \Phi_n \rangle = l + s$).

n	l	s	j
1	1	2	3
2	1	1	2
3	0	2	2
4	1	0	1
5	0	1	1
6	−1	2	1
7	1	−1	0
8	0	0	0
9	−1	1	0
10	1	−2	−1
11	0	−1	−1
12	−1	0	−1
13	0	−2	−2
14	−1	−1	−2
15	−1	−2	−3

Two of the cases in Fig. 8 concern what may be called a distortion-induced EFG due solely to the structural distortion from cubic symmetry.

The case of a moderately large axial distortion ($\Delta \gg |\delta| \gg |\lambda|, |h|$) may be considered by assuming $\lambda = h = 0$ in Eq. (5). With $\lambda = 0$ we may ignore the spin components of our basis functions. Our problem involves diagonalizing the perturbation $\frac{1}{3}\delta(L_z^2 - 2)$ within the basis (φ_1, φ_0, φ_{-1}) of Eqs. (9). We indicate the results on the left-hand side of Fig. 8. These results are obtained trivially because $(L_z^2 - 2)$ is already diagonal in this basis. The perturbation splits the ${}^5T_{2g}$ level into an orbital doublet and an orbital singlet separated by $|\delta|$. The expectation value $\langle \varphi_l | L_z^2 - 2 | \varphi_l \rangle$ is 1 for each doublet state and -2 for the singlet. If $\delta < 0$, the doublet will be lower, and at $T = 0\,^\circ$K the quadrupole splitting ΔE_Q will be positive. The sign of ΔE_Q and the order of the energy levels are reversed if $\delta > 0$.

Very similar results are obtained in the case of a small axial distortion ($|\delta| \ll |\lambda| \ll \Delta$; $h = 0$). We begin by considering only the perturbation $\lambda \vec{L} \cdot \vec{S}$. Diagonalization of the 15×15 matrix of $\lambda \vec{L} \cdot \vec{S}$ in the ${}^5T_{2g}$ basis yields a splitting into three levels as shown in the center of Fig. 8. For $\lambda < 0$, a triplet state is lowest. The diagonalization yields the following wave functions for this triplet:

$$\alpha_1 = (\tfrac{1}{10})^{1/2} \Phi_4 - (\tfrac{3}{10})^{1/2} \Phi_5 + (\tfrac{6}{10})^{1/2} \Phi_6 ,$$
$$\alpha_0 = (\tfrac{3}{10})^{1/2} \Phi_7 - (\tfrac{4}{10})^{1/2} \Phi_8 + (\tfrac{3}{10})^{1/2} \Phi_9 , \qquad (11)$$
$$\alpha_{-1} = (\tfrac{6}{10})^{1/2} \Phi_{10} - (\tfrac{3}{10})^{1/2} \Phi_{11} + (\tfrac{1}{10})^{1/2} \Phi_{12} .$$

Using these functions, we obtain

$$(L_z^2 - 2) = \begin{array}{c|ccc} & \alpha_1 & \alpha_0 & \alpha_{-1} \\ \hline \alpha_1 & 0.1 & 0 & 0 \\ \alpha_0 & 0 & -0.2 & 0 \\ \alpha_{-1} & 0 & 0 & 0.1 \end{array} . \qquad (12)$$

Thus, at $T = 0\,^\circ$K, $\langle L_z^2 - 2 \rangle = 0.1 - 0.2 + 0.1 = 0$: hence $\Delta E_Q = 0$. This result is to be expected as spin-orbit coupling does not destroy the cubic symmetry.

An axial distortion will break this symmetry. For $|\delta| \ll |\lambda|$, we may treat this problem by first-order perturbation theory applied within the α_l triplet. The results are identical to those obtained in the case of large $|\delta|$ except for reduction by a factor $\frac{1}{10}$.

The interesting special case of a magnetically induced EFG is illustrated at the far right of Fig. 8. We consider the situation in which $\delta = 0$ and the cubic symmetry is broken by turning on an exchange interaction hS_z, which corresponds to spin

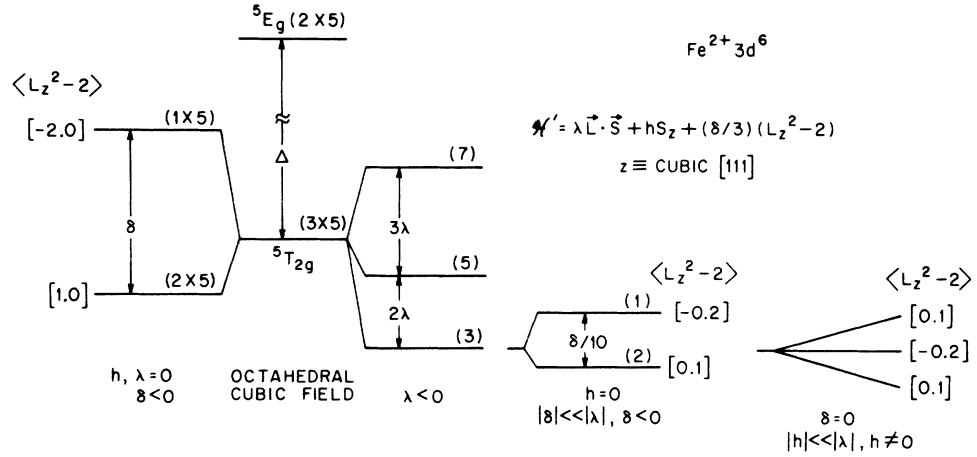

FIG. 8. Energy levels of Fe^{2+} ion acted on by octahedral cubic field and perturbation $\mathcal{H}'=\lambda\vec{L}\cdot\vec{S}+hS_z+\frac{1}{3}\delta(L_z^2-2)$ with z defined as the [111] cubic direction. Splitting of low-lying $^5T_{2g}$ levels is illustrated for various values of parameters in $\mathcal{H}'$. Numbers in parentheses are level degeneracies. Numbers in square brackets are expectation values $\langle L_z^2-2\rangle$ for the indicated states.

alignment along the [111] direction. In the α_l basis of Eq. (11) the representation of S_z is

$$S_z = \begin{array}{c|ccc} & \alpha_1 & \alpha_0 & \alpha_{-1} \\ \hline \alpha_1 & +1.5 & 0 & 0 \\ \alpha_0 & 0 & 0 & 0 \\ \alpha_{-1} & 0 & 0 & -1.5 \end{array} .$$

Thus, for $|h| \ll |\lambda|$ the interation hS_z will split the triplet into three levels having the expectation values of (L_z^2-2) indicated in Fig. 8. A nonzero EFG with ΔE_Q positive will result.

We now reconsider the spin direction question for $KFeF_3$. The choice in $\mathcal{H}'$ of spin alignment parallel to the distortion direction ensures satisfaction of the experimental finding $\eta=0$. However, if δ is so small that its effects are negligible, it is possible to satisfy $\eta=0$ by spin alignment parallel to a $\langle 100\rangle$ or $\langle 110\rangle$ direction of the cubic potential. (Directions other than $\langle 100\rangle$, $\langle 110\rangle$, or $\langle 111\rangle$ would yield $\eta\neq 0$.) With δ negligible, a magnetically induced EFG results. By diagonalization of $\mathcal{H}'$ with δ taken as zero and z redefined as a $\langle 100\rangle$ or $\langle 110\rangle$ direction, one may show that a negative $\langle L_z^2-2\rangle$ and hence a negative ΔE_Q is induced. Experimentally, ΔE_Q is positive for $KFeF_3$; hence, the spins must be aligned along a $\langle 111\rangle$ direction even if δ is negligibly small.

B. Fitting Procedure and Results

Our problem now is to find values for the various unknown parameters (λ, h, δ, $Q\langle r^{-3}\rangle_Q$, A, and $\langle r^{-3}\rangle_L$) such that the wave functions Ψ_n and energy levels E_n obtained by diagonalization of $\mathcal{H}'$ [Eq. (5)] will yield values of ΔE_Q [Eq. (6)] and $H_{\rm hf}^a$ [Eq. (7)] in agreement with experiment.

A complication in the fitting process is that δ and h both vary with temperature.

The axial splitting parameter δ must be zero above T_N, where $KFeF_3$ is cubic. Since the angular distortion $|90^\circ-\alpha|$ increases monotonically with decreasing temperature below T_N,[13] $|\delta|$ should behave similarly. A plausible assumption is the following:

$$\delta(T)=0\,, \qquad T>T_N$$
$$\delta(T)=\delta_0(1-T/T_N)^\gamma\,, \qquad T\leq T_N$$

where δ_0 and γ are constants to be determined by fitting the data. Many physical properties of a solid have been found to have a power-law dependence of this form in the vicinity of a critical point.

We determined the temperature dependence of h by the self-consistency condition of molecular-field theory. In the present case this requirement takes the following form: For any temperature T, the value of h inserted in $\mathcal{H}'$ must be such as to yield a value $\langle S_z\rangle$ at T satisfying

$$h(T)=12J\langle S_z\rangle. \tag{13}$$

If a particular value is assumed for λ and a particular form for $\delta(T)$, one may determine the self-consistent values of h graphically by the method[1] illustrated in Fig. 9. The curved lines are obtained by assuming various values for h, diagonalizing $\mathcal{H}'$ for each h value (and for each temperature if the assumed δ is temperature dependent), and using the results to calculate $\langle S_z\rangle$ at each temperature. The straight line represents Eq. (13).

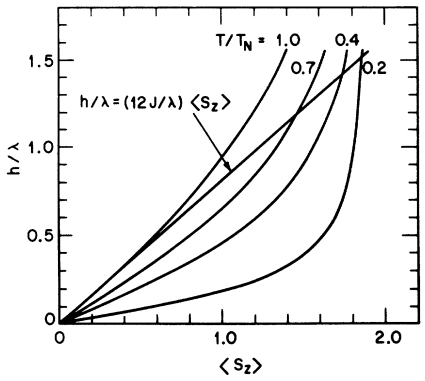

FIG. 9. Method used for determining self-consistent values of the exchange parameter h. These curves were calculated using the Hamiltonian $\mathcal{H}'$ of Eq. (5) with $\delta(T) = \delta_0(1 - T/T_N)^{1/2}$ and the parameters $\lambda = -50$ cm^{-1}, $\delta_0 = -35.5$ cm^{-1}, and $T_N = 112.51$ °K.

Its intersection with the h-vs-$\langle S_z\rangle$ curve for temperature T yields the self-consistent values of h and $\langle S_z\rangle$ at T. The slope of the straight line is determined by the requirement that the line be tangent at the origin to the h-vs-$\langle S_z\rangle$ curve for $T = T_N$. The value of J is obtained from the slope.

With T_N fixed at the value 112.51 °K determined by the power-law fit, we are left with six unknown parameters: λ, δ_0, γ, $Q\langle r^{-3}\rangle_Q$, A, and $\langle r^{-3}\rangle_L$.

A search for suitable values was made with the aid of a least-squares computer program which adjusted input guesses so as to minimize the differences between calculated and measured values of H_{hf} and ΔE_Q. The self-consistent values of h were determined in a subroutine which numerically simulated the graphical solution method. In these fits some of the data points near T_N were omitted in order to avoid overemphasis of data in this region, where molecular-field theory is known to be a poor approximation due to its neglect of spin correlations.[56] Only the following temperatures were considered: 37.97, 39.98, 50.06, 60.03, 69.98, 77.5, 86.05, 94.01, 100.00, 104.97, 110.07, and 112.51 °K.

The sign of H_{hf}^z has not been measured. Within the framework of restrictions to be described below, we were unable to fit the H_{hf} data with H_{hf}^z assumed positive. We therefore assumed that H_{hf}^z is negative in $KFeF_3$. This hypothesis is in agreement with a prediction made by Okiji and Kanamori on the basis of a theoretical analysis of hyperfine fields in a group of Fe^{2+} compounds.[59]

Restrictions on allowed values for the parameters were found necessary because of the large number of unknown parameters. Attempts to fit the data with all six parameters varying freely yielded for some of the parameters values which differed by more than a factor of 2 from those found in typical Fe^{2+} systems.

Our principal restriction was the requirement that the hyperfine parameter A not differ by more than about 10% from its value for FeF_2. This requirement seems reasonable in view of the similarity of the immediate Fe^{2+} surroundings in FeF_2 and $KFeF_3$.[26] In both cases there is an octahedron of fluoride ions (moderately distorted in the case of FeF_2). The Fe^{2+} site symmetry is orthorhombic in FeF_2, but the average Fe-F distance at room temperature (2.08 Å) is very close to the value of 2.06 Å for $KFeF_3$. The 4.2 °K CS relative to Fe foil is[36,60] 1.47 mm/sec for FeF_2 and 1.45 mm/sec for $KFeF_3$. This closeness indicates that the charge densities at the nuclei are nearly the same in the two cases. For FeF_2 Johnson and Ingalls[60] estimate a contact field of −518 kOe at 4.2 °K with $\langle S\rangle = 2$. This estimate yields $A \approx -260$ kOe. We therefore required -230 kOe $> A > -290$ kOe in our search.

An additional restriction was consideration only of the values 2, 1, $\frac{1}{2}$, $\frac{1}{3}$, and 0 for the exponent γ. This set permits a variety of physically plausible types of behavior for $\delta(T)$.

The shapes of curves calculated for H_{hf} vs T were quite sensitive to the value of λ. Shown in Fig. 10 are best-fit curves obtained with the constant A restricted as above, $\delta_0 = 0$, and three values of λ. With $|\lambda| = 40$ cm^{-1}, the calculated peak in H_{hf} is sharper than the observed peak. As $|\lambda|$ increases, the sharpness decreases. With $|\lambda| = 60$ cm^{-1} the peak in the calculated H_{hf} curve is nearly gone. Best-fit curves calculated with values of δ_0 comparable to our preliminary estimate did not differ very greatly from those with $\delta_0 = 0$. This point is illustrated by the similarity of the two curves in Fig. 11. Thus, we conclude that the H_{hf} data limit λ to the range

$$\lambda = -50 \pm 10 \text{ cm}^{-1},$$

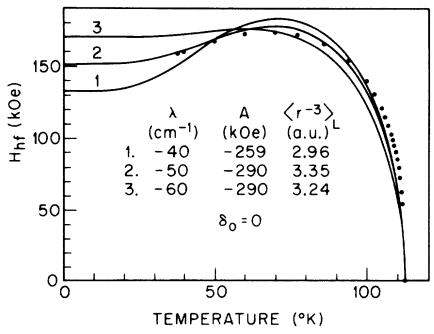

FIG. 10. Magnitude H_{hf} of measured hyperfine field for antiferromagnetic $KFeF_3$ (dots) and best-fit curves obtained assuming that A is restricted to range -260 ± 30 kOe, $\delta_0 = 0$, and the values indicated for λ. Values listed for A and $\langle r^{-3}\rangle_L$ provided the best fits.

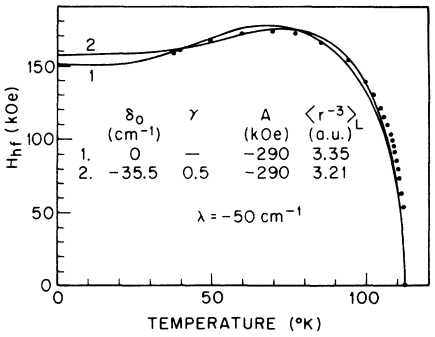

FIG. 11. Data for H_{hf} of antiferromagnetic $KFeF_3$ (dots) and best-fit curves obtained assuming $A = -260 \pm 30$ kOe, $\lambda = -50$ cm^{-1}, and either $\delta(T) = 0$ (curve 1) or $\delta(T) = \delta_0(1 - T/T_N)^{1/2}$ with $\delta_0 = -35.5$ cm^{-1} (curve 2). Values listed for A and $\langle r^{-3}\rangle_L$ provided the best fits. The poor quality of the fits near T_N reflects in part the neglect of many of the data points near T_N in the fitting process (see Sec. IV B).

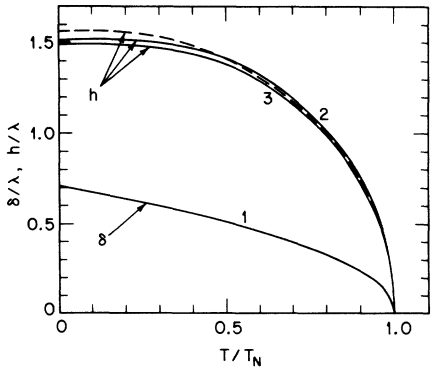

FIG. 13. Temperature dependence of parameters used in Fe^{2+} Hamiltonian $\mathcal{H}'$ [Eq. (5)] for several cases. Curve 1 is the temperature dependence of the axial distortion parameter $\delta(T)$ for our best fit: $\delta(T) = \delta_0(1 - T/T_N)^{1/2}$, $\delta_0 = -35.5$ cm^{-1}. Curve 2 is the self-consistent exchange parameter $h(T)$ obtained assuming $\lambda = -50$ cm^{-1} and this $\delta(T)$. Curve 3 is $h(T)$ obtained assuming $\lambda = -50$ cm^{-1} and $\delta(T) = 0$. The dashed line is the self-consistent $h(T)$ obtained by use of the Brillouin function for spin 2. All quantities are plotted in units of $\lambda = -50$ cm^{-1}.

but do not restrict the form of $\delta(T)$.

In contrast, the shapes of calculated curves of ΔE_Q vs T were found to be quite dependent on assumptions regarding δ_0 and γ, but not significantly affected by the value assigned to λ for λ in the range -50 ± 10 cm^{-1}. We therefore used the ΔE_Q data to search for suitable δ_0 and γ values with λ fixed at -50 cm^{-1}.

To test the magnetically induced EFG hypothesis, we first considered the case $\delta_0 = 0$. The best fit is shown in Fig. 12 by the inflected line (curve 1), a rather poor representation of the data.

Similar inflected curves were obtained with

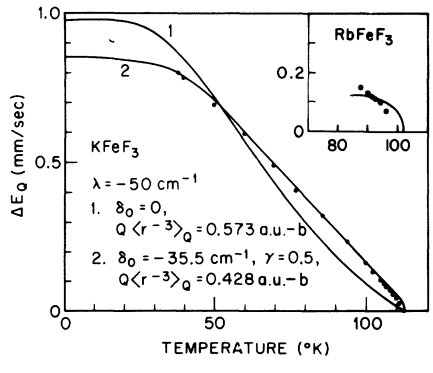

FIG. 12. Data for ΔE_Q of antiferromagnetic $KFeF_3$ (dots) and best-fit curves obtained assuming $\lambda = -50$ cm^{-1} and either $\delta(T) = 0$ (curve 1) or $\delta(T) = \delta_0(1 - T/T_N)^{\gamma}$ (curve 2). Values listed for $Q\langle r^{-3}\rangle_Q$ and for δ_0 and γ of curve 2 provided the best fits. (Some of the data points near T_N have been omitted for clarity.) Inset: Data for antiferromagnetic $RbFeF_3$ (from Ref. 3) and fit obtained using $T_N = 102$ °K, $\delta_0 = -68.7$ cm^{-1}, and the λ, γ, and $Q\langle r^{-3}\rangle_Q$ values of curve 2.

$\delta_0 \neq 0$ and γ fixed at 2 and 1. With $\delta_0 \neq 0$ and $\gamma = 0$, the fit was also poor. The calculated ΔE_Q has a large step at T_N, reflecting the fact that $\delta(T)$ is a step function for this case.

However, good fits were obtained with $\delta_0 \neq 0$ and $\gamma = \frac{1}{2}$ or $\frac{1}{3}$. The fit was slightly better with $\gamma = \frac{1}{2}$. This result is shown by curve 2 in Fig. 12. The value of δ_0 which gave the best fit was -35.5 cm^{-1}. The values found for λ, A, $\langle r^{-3}\rangle_L$, and $\langle r^{-3}\rangle_Q$ are listed in column 1 of Table IV. (We assume[51] $Q = 0.21b$ to obtain $\langle r^{-3}\rangle_Q$.)

V. DISCUSSION

A. Some Comparisons

Several comparisons are instructive at this point. In Fig. 13 we illustrate the relative sizes of $\delta(T)$ and $h(T)$. At 78 °K, $|\delta| = 19.7$ cm^{-1}, about one-half of our preliminary estimate based on G_{ij}. Also shown are $h(T)$ curves calculated with and without the presence of a crystal field. These indicate the slightness of the influence of the crystal field here on the temperature dependence of the sublattice magnetization. The crystal field also has little effect on the value derived for J. With the crystal field neglected, we would obtain $J = -3.26$ cm^{-1} [by Eq. (8)]. Our best fits to both the cubic and noncubic cases yielded $J = -3.38$ cm^{-1}.

The effect of $\delta(T)$ on the energy levels of the ion is illustrated in Fig. 14. The energy levels as a function of temperature for the noncubic case are shown in the top portion of Fig. 14. In the bottom portion we show the low-lying levels obtained as-

TABLE IV. Parameters ascribed to Fe^{2+} ion in various situations.

	$KFeF_3$ (this work)	$CoO:Fe^{2+}$ [a]	$KMgF_3:Fe^{2+}$ [b]	$MgO:Fe^{2+}$ [b]	$FeSiF_6 \cdot 6H_2O$ [c]	FeF_2 [d]	Free ion	$KFeF_3$ [e] (theory)
λ (cm^{-1})	−50	−71	−60	−50	−90	−85	−103 [f]	−90
A (kOe)	−290	−234	−248	−230	−210	−259	−275 [g]	...
$\langle r^{-3}\rangle_L$ (a.u.)	3.21	4.4	4.1	3.0	3.5	3.0	4.59 [g]	4.01
$\langle r^{-3}\rangle_Q$ (a.u.) [h]	2.04	3.0	4.1	3.0	3.5	3.0	4.93 [g]	4.31

[a] Reference 61.
[b] Reference 62.
[c] Reference 51 and 63.
[d] Reference 60.
[e] These are obtained from the free-ion values (preceding column) using the covalency reduction factor of 0.874 calculated in Ref. 64.
[f] Reference 40.
[g] Reference 45.
[h] Values for $\langle r^{-3}\rangle_Q$ are based on $Q = 0.21b$ (Ref. 51).

suming cubic symmetry. The chief difference is the level crossing at about 45 °K which occurs only for the cubic case.

In Table V we summarize for the noncubic (a) and cubic (b) cases some properties at $T = 0$ °K of the three lowest states. It is interesting to note that, qualitatively, the ground states are quite similar and the excited-state pairs also match quite well provided one takes the level inversion into account. This similarity was also found to hold at higher temperatures. Thus, the qualitative difference in the shape of ΔE_Q vs T for the two cases is not related to any gross qualitative differences in the properties of the individual states.

The data assembled in Table IV facilitate checking on the plausibility of the parameters required to fit our $KFeF_3$ measurements to our model. In addition to summarizing our best-fit values, Table IV contains in columns 2–6 some parameters assigned to Fe^{2+} on the basis of fits to other experiments.[51,60–63] These fits involved the crystal-field and molecular-field models and, in most cases, the approximation $\langle r^{-3}\rangle_L = \langle r^{-3}\rangle_Q$. In column 7 we list free-ion values. The value for λ is based on experiment,[40] while the values for A, $\langle r^{-3}\rangle_L$, and $\langle r^{-3}\rangle_Q$ were calculated by Freeman and Watson using the unrestricted Hartree-Fock formalism.[45] The numbers in the last column were obtained by assuming λ, $\langle r^{-3}\rangle_L$, and $\langle r^{-3}\rangle_Q$ to be reduced from these free-ion values by a covalency reduction factor of 0.874. This value was calculated for $KFeF_3$ by Silva and Ingalls[64] on the basis of a configuration-interaction computation of wave functions for the $(FeF_6)^{4-}$ cluster.

Table IV indicates that our values for λ, A, and $\langle r^{-3}\rangle_L$ for Fe^{2+} in $KFeF_3$ are not unreasonable. For each of these parameters, at least one of the other compounds has been assigned a value within 10% of our value.

While our value for $\langle r^{-3}\rangle_Q$ differs considerably from the others in the table, it is fairly close to values assigned by Hazony[65] for Fe^{2+} in $FeTiO_3$, $FeCl_2$, $FeBr_2$ and FeI_2. Hazony obtained $\langle r^{-3}\rangle_Q$ values between 1.7 and 2.4 a.u. from the saturation value of ΔE_Q in the paramagnetic state of each of these materials.

Our finding of a large difference between $\langle r^{-3}\rangle_Q$ and $\langle r^{-3}\rangle_L$ is somewhat surprising in view of the frequent assumption that $\langle r^{-3}\rangle_Q = \langle r^{-3}\rangle_L$.[59,60,62,63] However, such a finding is not unprecedented. A similar difference was obtained in a fit to $CoO:Fe^{2+}$ data (column 2). These differences are substantially larger than one would expect to arise from error due to neglect of the lattice EFG and therefore suggest that the assumption of equality between $\langle r^{-3}\rangle_Q$ and $\langle r^{-3}\rangle_L$ needs reexamination.

Another noteworthy difference is the one between our parameter values and those obtained using the covalency reduction factor calculated by Silva and Ingalls (column 8). This discrepancy

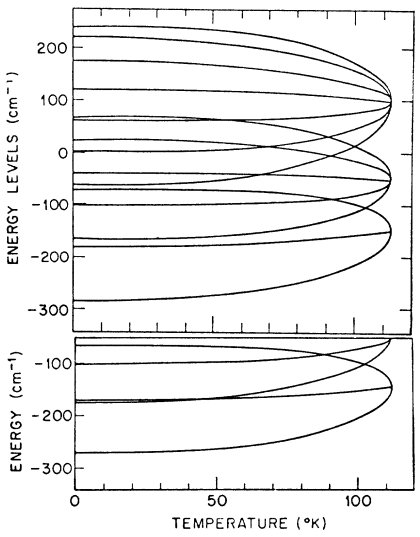

FIG. 14. Temperature dependence of Fe^{2+} energy levels for two cases. Top: $\lambda = -50$ cm^{-1}, $\delta(T) = \delta_0(1 - T/T_N)^{1/2}$, $\delta_0 = -35.5$ cm^{-1}. Bottom: $\lambda = -50$ cm^{-1}, $\delta(T) = 0$. Only the five lowest levels are shown for the second case.

suggests that other reduction mechanisms are operative.[66]

B. Implications for $RbFeF_3$

Mössbauer spectra for antiferromagnetic tetragonally distorted $RbFeF_3$ indicate $\Delta E_Q > 0$ and appear to be consistent with $\eta = 0$ and $\vec{H}_{hf}$ parallel to the principal axis of V_{ij}.[3-5] If we assume the EFG to be magnetically induced, then only spin alignment along a $\langle 111 \rangle$ direction is consistent with these properties.

However, the hypothesis $\delta = 0$ is not reasonable for $RbFeF_3$. The magnetoelastic tensor G_{ij} for Fe^{2+} in $KMgF_3$ and the distortion observed in $RbFeF_3$ yield $|\delta| \approx 100 \pm 12$ cm^{-1} at 86 °K.[67] A sizable nonzero value for δ in $RbFeF_3$ implies that the spins must align parallel to the $\langle 100 \rangle$ distortion for consistency with $\eta = 0$.

We may analyze this case with the Hamiltonian $\mathcal{H}'$ of Eq. (5) provided we redefine z to be the [100] direction. An appropriate set of basis functions would again be of the form $\varphi_l \chi_s$, but now, with $z \equiv [100]$, the functions φ_l are[42]

$$\varphi_1 = d_{-1} ,$$

$$\varphi_0 = (\tfrac{1}{2})^{1/2}(d_2 - d_{-2}) ,$$

$$\varphi_{-1} = -d_1 .$$

With these basis functions, matrix elements of $\vec{L}$ and $\vec{S}$ are identical to those of the trigonal ($z \equiv [111]$) case. Matrix elements of $(L_z^2 - 2)$ are equal in magnitude but opposite in sign to the values for the trigonal case [Eq. (10)]; i.e., for the tetragonal ($z \equiv [100]$) case

$$(L_z^2 - 2) = \begin{array}{c|ccc} & \varphi_1 & \varphi_0 & \varphi_{-1} \\ \hline \varphi_1 & -1 & 0 & 0 \\ \varphi_0 & 0 & 2 & 0 \\ \varphi_{-1} & 0 & 0 & -1 \end{array} .$$

It follows that by itself an exchange field parallel to [100] yields $\Delta E_Q < 0$ while a [100] distortion by itself will yield $\Delta E_Q < 0$ if $\delta > 0$ and $\Delta E_Q > 0$ if $\delta < 0$. Since ΔE_Q is positive in $RbFeF_3$, δ must be negative, and the effects of the distortion term in $\mathcal{H}'$ must outweigh those of the exchange term.

The Mössbauer data currently available[3-5] for the antiferromagnetic region of $RbFeF_3$ are for powder samples and cover a relatively small temperature range: from $T_N = 102$ °K down to the structural transition at ~86 °K. Hence a fitting procedure as complex as that we have used for $KFeF_3$ is not justified.

To determine the approximate size of δ needed to account for the quadrupole splitting measured in $RbFeF_3$, we used a simpler procedure. We employed the Hamiltonian $\mathcal{H}'$ with z taken as the [100] direction and with $h(T)$ obtained by use of the Brillouin function for spin 2. We took $T_N = 102$ °K from Ref. 3 and adopted the values $\gamma = \frac{1}{2}$, $\lambda = -50$ cm^{-1}, and $Q\langle r^{-3}\rangle_Q = 0.428$ a.u. $- b$ from our best fit for

TABLE V. Properties at $T = 0$ °K of the three lowest-lying states of Fe^{2+} for two cases. Case (a) corresponds to the noncubic case (curve 2, Figs. 11 and 12); case (b) corresponds to the cubic case (curve 1, Figs. 11 and 12). The functions Φ_n are specified in Table III.

	(a)			(b)		
m	1	2	3	1	2	3
E_m (cm^{-1})	−288	−183	−167	−277	−181	−178
$\langle J_z \rangle_m$[a]	1	0	2	1	2	0
$\langle S_z \rangle_m$	1.88	0.72	1.77	1.84	1.83	0.64
$\langle L_z \rangle_m$	0.88	0.72	−0.23	0.84	−0.17	0.64
$\langle h_z^D \rangle_m$[b]	−2.40	−0.39	4.51	−2.03	5.24	−0.20
$\langle L_z^2 - 2 \rangle_m$	0.69	0.40	−1.31	0.59	−1.49	0.21
H_C (kOe)	−545	−209	−513	−534	−531	−186
H_L(kOe)	354	290	−93	352	−71	268
H_D (kOe)	34	6	−65	30	−79	3
ΔE_Q (mm/sec)	0.85	0.49	−1.62	0.98	−2.47	0.35
Ψ_1	$0.100\Phi_4 - 0.320\Phi_5 + 0.942\Phi_6$			$0.116\Phi_4 - 0.371\Phi_5 + 0.922\Phi_6$		
Ψ_2	$0.198\Phi_7 - 0.449\Phi_8 + 0.871\Phi_9$			$-0.412\Phi_2 + 0.911\Phi_3$		
Ψ_3	$-0.480\Phi_2 + 0.877\Phi_3$			$0.219\Phi_7 - 0.512\Phi_8 + 0.831\Phi_9$		

[a] $J_z \equiv -L_z + S_z$.

[b] $h_z^D \equiv 4S_z - (\vec{L}\cdot\vec{S})\,L_z - L_z\,(\vec{L}\cdot\vec{S})$.

$KFeF_3$. Varying only δ_0, we obtained the best fit to the data points of Ref. 3 with $\delta_0 = -68.7\ cm^{-1}$, about twice the value found for $KFeF_3$.

The quality of this fit (inset, Fig. 12) is considerably poorer than that of our $KFeF_3$ fit. It is not clear whether this result is due to inadequacies in the data, the model, or the abbreviated fitting procedure. Although little significance can be attributed to the parameter values found, this calculation does demonstrate that an η value of zero and a ΔE_Q of the appropriate sign and order of magnitude can be obtained with $\langle 100 \rangle$ spin alignment and a plausible value for δ_0.

C. Cubic-to Axial Transition

Our result for the axial distortion parameter in $RbFeF_3$ is inconsistent with a proposed explanation of the cubic-to-axial phase transition.

Goodenough *et al.*[11] have attributed the transitions of $KFeF_3$ and $RbFeF_3$ to Jahn-Teller stabilization effects in the presence of internal (exchange fields. For distortion occurring at T_N, their model requires that δ have the sign which would cause a doublet ground state (with spin-orbit effects included) in the absence of the exchange field.

We have already noted that with $\delta = h = 0$, $\mathcal{H}'$ yields a ground triplet (α_1, α_0, α_{-1}) [Eq. (11)] for Fe^{2+}. For the trigonal case the matrix elements of $(L_z^2 - 2)$ within this triplet are given by the matrix of Eq. (12). This matrix indicates δ must be negative to obtain the doublet ground state $\alpha_{\pm 1}$. Since $\langle \alpha_{\pm 1} | L_z^2 - 2 | \alpha_{\pm 1} \rangle$ is positive, a positive ΔE_Q results, in agreement with experiment for $KFeF_3$.

On the other hand, for the tetragonal case the matrix elements of $(L_z^2 - 2)$ are of opposite sign within the ground spin-orbit triplet. Therefore, the doublet ground state required by the Jahn-Teller model is obtained with $\delta > 0$. This sign for δ is opposite to that needed to account for the observed sign of ΔE_Q in $RbFeF_3$.

VI. SUMMARY AND CONCLUSIONS

Mössbauer absorption spectra of ^{57}Fe in $KFeF_3$ reflect the existence of three structurally and magnetically distinct phases between 297 and 4.2 °K. On the basis of Mössbauer, x-ray, magnetic, and neutron-diffraction studies, we may characterize these phases as follows:

I ($T_N < T \leq 297$ °K) simple cubic perovskite-structure paramagnet.

II ($T_R < T \leq T_N$) trigonal antiferromagnet.

III ($4.2° \leq T \leq T_R$) weak ferromagnet with a structure of symmetry lower than trigonal.

Analysis of Mössbauer spectra of an unstrained single crystal of $KFeF_3$ establishes the following: (a) $T_N = 112.5 \pm 0.5$ °K; (b) $T_R = 36.6 \pm 0.5$ °K; (c) in the antiferromagnetic phase the spins align parallel to the $\langle 111 \rangle$ distortion direction; (d) in contrast to a finding in a Mössbauer study of powder $KFeF_3$, there is no slowing of the Fe^{2+} relaxation rate near T_N.

Spectra of a strained single crystal show that stress can raise the value of T_N and cause rotation of the spin directions.

The temperature dependence of H_{hf} and ΔE_Q in the antiferromagnetic state of $KFeF_3$ is in poor agreement with predictions of the magnetically induced EFG model. Good agreement with the $KFeF_3$ data can be obtained by augmenting the Hamiltonian of this model by a trigonal crystal-field term $(\frac{1}{3}\delta)(L_z^2 - 2)$, where δ vanishes above T_N and varies below T_N as $(1 - T/T_N)^{\gamma}$ with $\gamma = \frac{1}{2}$ or $\frac{1}{3}$. Our optimum fit yields a value of δ about one-half that predicted on the basis of the magnetoelastic tensor G_{ij} of Fe^{2+} in $KMgF_3$ and values for λ, $\langle r^{-3} \rangle_L$, and $\langle r^{-3} \rangle_Q$ in reasonable agreement with those characteristic of Fe^{2+} in other compounds.

The hypothesis that there is a comparably large δ in $RbFeF_3$ and the observation $\eta = 0$ lead to the conclusion that the spins in $RbFeF_3$ align parallel to the $\langle 100 \rangle$ distortion. This result is in disagreement with the $\langle 111 \rangle$ alignment direction predicted by use of the magnetically induced EFG model. With $\langle 100 \rangle$ spin alignment the sign required for the axial distortion parameter in $RbFeF_3$ is opposite to that predicted by a model which attributes the cubic-to-axial transformation to Jahn-Teller stabilization effects.

Note added in proof. Recently, F. Varret and P. Imbert published a study of a stressed $KFeF_3$ single crystal [Phys. Status Solidi B56, 127 (1973)]. Their results support our conclusion that the Fe^{2+} spins in $KFeF_3$ align parallel to a $\langle 111 \rangle$ direction.

ACKNOWLEDGMENTS

We thank J. J. Hurst, Jr. and C. Fortunka for communication of results of their x-ray measurements on $KFeF_3$, L. Holmes for communication of the magnetization data, and W. F. Flood for technical assistance. We are grateful to M. D. Sturge for several helpful discussions and for acquainting us with properties of the magnetoelastic tensor. We have also benefited from discussions with M. E. Caspari, M. G. Clark, M. E. Lines, and G. K. Wertheim.

*Part of the work by this author was performed at the Physics Dept., University of Pennsylvania, with support by the Office of Naval Research.

†Present address: Argonne National Laboratory, Argonne, Ill. 60439.

[1] R. Fatehally, G. K. Shenoy, N. P. Sastry, and R. Nagarajan, Phys. Lett. A **25**, 453 (1967); R. Fatehally, N. P. Sastry, and R. Nagarajan, Phys. Status Solidi **26**, 91 (1968).

[2] U. Ganiel, M. Malamud, and S. Shtrikman, Bull. Am. Phys. Soc. **14**, 133 (1969).

[3]G. K. Wertheim, H. J. Guggenheim, H. J. Williams, and D. N. E. Buchanan, Phys. Rev. **158,** 446 (1967); and J. Appl. Phys. **39,** 1253 (1968).
[4]G. R. Hoy and S. Chandra, J. Chem. Phys. **47,** 961 (1967).
[5]U. Ganiel, M. Kestigan, and S. Shtrikman, Phys. Lett. A **24,** 577 (1967).
[6]U. Ganiel and S. Shtrikman, Phys. Rev. **167,** 258 (1968).
[7]This model has had widespread application in discussion of EFG's observed at Fe^{2+} nuclei in cubic or nearly cubic magnetically ordered systems. Reference 6 presents a detailed exposition. In addition to $KFeF_3$ and $RbFeF_3$, materials considered have included the following: Fe^{++}:NiO and Fe^{++}:MnO [J. D. Siegwarth, Phys. Rev. **155,** 285 (1967)]; $FeCr_2S_4$ [M. Eibschütz, S. Shtrikman, and Y. Tenenbaum, Phys. Lett. A **24,** 563 (1967); G. R. Hoy and K. P. Singh, Phys. Rev. **172,** 514 (1968); M. R. Spender and A. H. Morrish, Can. J. Phys. **50,** 1125 (1972)]; and $Cd_{0.98}Fe_{0.002}Cr_2S_4$ [A. M. van Diepen and R. P. van Stapele, Phys. Rev. B **5,** 2462 (1972)].
[8]J. K. Wigmore, H. M. Rosenberg, and D. K. Garrod, J. Appl. Phys. **39,** 682 (1968).
[9]The magnetoelastic tensor G_{ij} relates the energy splitting of a degenerate ground state to the strain causing the splitting. For an introductory discussion of G_{ij}, see E. R. Feher, Phys. Rev. **136,** A145 (1964).
[10]Details of these estimates are presented in Secs. IV A and VB.
[11]J. B. Goodenough, N. Menyuk, K. Dwight, and J. A. Kafalas, Phys. Rev. B **2,** 4640 (1970).
[12]R. L. Martin, R. S. Nyholm, and N. C. Stephenson, Chem. Ind. (Lond.) 83 (1956).
[13]A. Okazaki, Y. Suemune, and T. Fuchikami, J. Phys. Soc. Jap. **14,** 1823 (1959); A. Okazaki and Y. Suemune, J. Phys. Soc. Jap. **16,** 671 (1961).
[14]K. Knox, Acta Crystallogr. **14,** 583 (1961).
[15]Franklin F. Y. Wang and M. Kestigan, J. Appl. Phys. **37,** 975 (1966).
[16]L. R. Testardi, H. J. Levinstein, and H. J. Guggenheim, Phys. Rev. Lett. **19,** 503 (1967).
[17]Franklin F. Y. Wang, D. E. Cox, and M. Kestigan, Phys. Rev. B **3,** 3946 (1971).
[18]K. Hirakawa, K. Hirakawa, and T. Hashimoto, J. Phys. Soc. Jap. **15,** 2063 (1960).
[19]D. J. Machin, R. L. Martin, and R. S. Nyholm, J. Chem. Soc. (Lond.) 1490 (1963).
[20]V. Scatturin, L. Corliss, N. Elliot, and J. Hastings, Acta Crystallogr. **14,** 19 (1961).
[21]H. J. Levinstein, H. J. Guggenheim, and C. D. Capio, Trans. AIME (Am. Inst. Min. Metall. Pet. Eng.) **245,** 365 (1969); E. M. Gyorgy, H. J. Levinstein, J. F. Dillon, Jr., and H. J. Guggenheim, J. Appl. Phys. **40,** 1599 (1969).
[22]Model 118L, Rosemount Engineering Co., Minneapolis, Minn.
[23]Model MHSP2406, Series II, Solitron Devices, Inc., Riviera Beach, Fla.
[24]R. L. Cohen, P. G. McMullin, and G. K. Wertheim, Rev. Sci. Instrum. **34,** 671 (1963); R. L. Cohen, Rev. Sci. Instrum. 37, 260 (1966); Rev. Sci. Instrum. 37, 957 (1966).
[25]C. E. Violet and D. N. Pipkorn, J. Appl. Phys. **42,** 4339 (1971).
[26]H. K. Perkins and Y. Hazony, Phys. Rev. B **5,** 7 (1972).
[27]G. K. Wertheim, *Mössbauer Effect: Principles and Applications* (Academic, New York, 1964).
[28]M. H. Cohen and F. Reif, Solid State Phys. **5,** 321 (1957).
[29]These results are easily derived by summation of the appropriate intensity formulas for the directions involved. For these formulas, see Ref. 27, p. 75.
[30]S. V. Karyagin, Fiz. Tverd. Tela. 8, 493 (1966) [Sov. Phys.-Solid State 8, 391 (1966)].
[31]G. R. Davidson, Nucl. Instrum. Methods **107,** 557 (1973).
[32]The intervals $0 \leq \theta \leq 90°$ and $0 \leq \phi \leq 90°$ are sufficient since calculated excited-state energies are unaffected by substitution of $(180° - \theta)$ for θ or $(180° \pm \phi)$ for θ.
[33]J. J. Hurst, Jr. and C. Fortunka (private communication).
[34]L. Holmes (private communication).
[35]G. K. Wertheim, H. J. Guggenheim, H. J. Levinstein, D. N. E. Buchanan, and R. C. Sherwood, Phys. Rev. **173,** 614 (1968).
[36]G. K. Wertheim and D. N. E. Buchanan, Phys. Rev. **161,** 478 (1967).
[37]For discussion of relaxation effects in Mössbauer spectroscopy, see F. van der Woude and A. J. Dekker, Phys. Status Solidi **9,** 775 (1965); and M. Blume and J. A. Tjon, Phys. Rev. **165,** 446 (1968).
[38]The strong magnetoelastic interactions in $KFeF_3$ are reminiscent of those in $RbFeF_3$. See Ref. 21.
[39]W. Low and M. Weger, Phys. Rev. **118,** 1119 (1960).
[40]R. E. Trees, Phys. Rev. **82,** 683 (1951).
[41]G. D. Jones, Phys. Rev. **155,** 259 (1967).
[42]B. Bleaney and K. W. H. Stevens, Rep. Prog. Phys. **16,** 108 (1953).
[43]The expression used to represent effects of the trigonal distortion is based on the operator equivalent (Ref. 42) $[3L_z^2 - L(L+1)]$ for $(3z^2 - r^2)$ and on neglect of the fourth-order trigonal-field term.
[44]R. Ingalls, Phys. Rev. **133,** A787 (1964).
[45]R. E. Watson and A. J. Freeman, in *Hyperfine Interactions*, edited by A. J. Freeman and R. B. Frankel (Academic, New York, 1967).
[46]R. Ingalls, Phys. Rev. **128,** 1155 (1962).
[47]R. M. Sternheimer, Phys. Rev. **130,** 1423 (1963).
[48]A. J. Nozik and M. Kaplan, Phys. Rev. **159,** 273 (1967).
[49]M. Eibschütz, U. Ganiel, and S. Shtrikman, Phys. Rev. **151,** 245 (1966); M. Eibschütz, U. Ganiel, and S. Shtrikman, Phys. Rev. **156,** 259 (1967); U. Ganiel and S. Shtrikman, Phys. Rev. **177,** 503 (1969).
[50]We assume the electronic relaxation time to be short in comparison with the nuclear precession time. See Ref. 37.
[51]R. Ingalls, Phys. Rev. **188,** 1045 (1969).
[52]For a discussion of the supertransferred hyperfine field see N. L. Huang, R. Orbach, E. Simánek, J. Owen, and D. R. Taylor, Phys. Rev. **156,** 383 (1967). Since this field is approximately proportional to $\langle S_z \rangle$, we cannot separate it from the contact field.
[53]Although $\langle r^{-3} \rangle_L$ and $\langle r^{-3} \rangle_D$ may differ by 10% (Ref. 45), this is a reasonable approximation since the dipolar field usually makes a small contribution to the total hyperfine field.
[54]J. Owen, Proc. R. Soc. A **227,** 183 (1955).
[55]F. S. Ham, Phys. Rev. **138,** A1727 (1965); F. S. Ham, W. M. Schwarz, and M. C. M. O'Brien, Phys. Rev. **185,** 548 (1969).
[56]J. S. Smart, *Effective Field Theories of Magnetism* (Saunders, Philadelphia, Pa., 1966).
[57]See J. F. Nye, *Physical Properties of Crystals* (Oxford U. P., London, 1960), Chap. 6, for the definition of ϵ_{12}.
[58]S. Sugano, Y. Tanabe, and H. Kamimura, *Multiplet Structure of Transition-Metal Ions in Crystals* (Academic, New York, 1970), p. 132.
[59]A. Okiji and J. Kanamori, J. Phys. Soc. Jap. **19,** 908 (1964).
[60]D. P. Johnson and R. Ingalls, Phys. Rev. B **1,** 1013 (1970).
[61]H. N. Ok and J. G. Mullen, Phys. Rev. **168,** 563 (1968).
[62]R. B. Frankel, J. Chappert, J. R. Regnard, A. Misetich, and C. R. Abeledo, Phys. Rev. B **5,** 2469 (1972).
[63]C. E. Johnson, Proc. Phys. Soc. Lond. **92,** 748 (1967).
[64]D. M. Silva and R. Ingalls, Phys. Rev. B **5,** 3725 (1972).
[65]Y. Hazony, Phys. Rev. B **3,** 711 (1971).
[66]A possible cause of the large reduction in λ may be the dynamic Jahn-Teller effect. The low λ values for Fe^{2+} in $KMgF_3$ and MgO have been attributed to this effect. See

Refs. 55 and 62.

[67]For a distortion along [100] accompanied by a fractional volume change $\Delta V/V$, $\delta = 7.5G_{11}[-3(c-a)/a + \Delta V/V]$. The value for $|\delta|$ in the text is obtained with $(c-a)/a$ and $\Delta V/V$ from Ref. 16 and $|G_{11}|$ from Ref. 8.